

NRC Publications Archive Archives des publications du CNRC

The large gap E-plane Omori circulator: first and second circulation conditions

Helszajn, Joseph; Carignan, Louis-Philippe; McKay, Mark; Tsounis, Bill; Wu, Ke

This publication could be one of several versions: author's original, accepted manuscript or the publisher's version. / La version de cette publication peut être l'une des suivantes : la version prépublication de l'auteur, la version acceptée du manuscrit ou la version de l'éditeur.

For the publisher's version, please access the DOI link below. / Pour consulter la version de l'éditeur, utilisez le lien DOI ci-dessous.

Publisher's version / Version de l'éditeur:

<https://doi.org/10.1049/mia2.70026>

IET Microwaves, Antennas & Propagation, 19, 1, 2025-05-15

NRC Publications Archive Record / Notice des Archives des publications du CNRC :

<https://nrc-publications.canada.ca/eng/view/object/?id=ac78fc30-9476-4f52-a30d-e93787d38361>

<https://publications-cnrc.canada.ca/fra/voir/objet/?id=ac78fc30-9476-4f52-a30d-e93787d38361>

Access and use of this website and the material on it are subject to the Terms and Conditions set forth at

<https://nrc-publications.canada.ca/eng/copyright>

READ THESE TERMS AND CONDITIONS CAREFULLY BEFORE USING THIS WEBSITE.

L'accès à ce site Web et l'utilisation de son contenu sont assujettis aux conditions présentées dans le site

<https://publications-cnrc.canada.ca/fra/droits>

LISEZ CES CONDITIONS ATTENTIVEMENT AVANT D'UTILISER CE SITE WEB.

Questions? Contact the NRC Publications Archive team at

PublicationsArchive-ArchivesPublications@nrc-cnrc.gc.ca. If you wish to email the authors directly, please see the first page of the publication for their contact information.

Vous avez des questions? Nous pouvons vous aider. Pour communiquer directement avec un auteur, consultez la première page de la revue dans laquelle son article a été publié afin de trouver ses coordonnées. Si vous n'arrivez pas à les repérer, communiquez avec nous à PublicationsArchive-ArchivesPublications@nrc-cnrc.gc.ca.

ORIGINAL RESEARCH OPEN ACCESS

The Large Gap E-Plane Omori Circulator: First and Second Circulation Conditions

 Joseph Helszajn^{1†} | Louis-Philippe Carignan²  | Mark McKay³ | Bill Tsounis⁴ | Ke Wu⁵

¹Heriot-Watt University, Edinburgh, Scotland | ²Digital Technologies, Computer Vision and Graphics, National Research Council Canada, Montreal, Canada | ³Leonardo UK Ltd, Edinburgh, Scotland | ⁴Apollo Microwaves, Dorval, Canada | ⁵Polytechnique Montreal, PolyGrames Research Center, Montréal, Canada

Correspondence: Louis-Philippe Carignan (louis-philippe.carignan@nrc-cnrc.gc.ca)

Received: 26 May 2024 | **Revised:** 26 April 2025 | **Accepted:** 29 April 2025

Handling Editor: Yongle Wu

Funding: The authors received no specific funding for this work.

Keywords: circulators | ferrite circulators | ferrite devices

ABSTRACT

A characteristic of the E-plane circulator is that it displays two neighbouring solutions for the first and second circulation conditions. The so-called small gap E-plane circulator was dealt with in the literature. This paper is concerned with the large gap geometry. It outlines a simple eigenvalue subroutine for the design of either arrangement, and includes some experimental data in WR75 waveguide for the degree-one large gap geometry. Good agreement was found between numerical simulations and experiments. High peak power analysis showed a significant improvement for large gap E-plane geometry, in comparison to the small gap E-plane as well as the H-plane junction circulator.

1 | Introduction

The E-plane junction circulator is devised by placing one or two quarter-wave long gyromagnetic resonators on the narrow wall of a waveguide 3-port junction [1–5]. A large gap between ferrite resonators, in addition to operating above resonance, may support megawatt peak power handling capability [6–10]. Further, a dielectric sleeve [8, 11] or a quarter-wave transformer can be used to increase the bandwidth of the E-plane circulator, and a radial composite resonator may be used to increase the average power handling [10, 12].

Field theory, mode charts and equivalent circuits of the E-plane circulator were established in Refs. [13–30]. The use of full-wave simulation tools, such as CST Microwave Studio or HFSS, for instance, allows for more complex geometry-shaped circulators to be considered. Razavipour et al. designed a double band E-

plane circulator by adjusting the dimensions of the ferrite resonators [31]. Deng et al. designed a four-port E-plane circulator using X-shaped ferrite disks and a septum [32]. The same authors designed a four-port differential phase shift circulator where the ferrite slabs are sitting on the broad wall of waveguide [33].

A fundamental characteristic of the E-plane junction is that it displays two neighbouring solutions for the first and second circulation conditions [27].

The first, a so-called small gap, has a passband about its mid-band frequency. The second, a so-called large gap solution, because the distance between the ferrite resonators is usually larger than that of the small gap counterpart, has a stopband. The former was discussed in Ref. [27] and the second is the object of this work. The prevailing solution depends upon whether the in-phase eigenvalue is either in-phase or 180° out-

[†]Deceased.

This is an open access article under the terms of the [Creative Commons Attribution](https://creativecommons.org/licenses/by/4.0/) License, which permits use, distribution and reproduction in any medium, provided the original work is properly cited.

© 2025 The Author(s). *IET Microwaves, Antennas & Propagation* published by John Wiley & Sons Ltd on behalf of The Institution of Engineering and Technology.

of-phase with the degenerate counter-rotating eigenvalues at the reference planes of the junction.

The paper is divided as follows. We present the geometry of the E-plane circulator under study in Section 2. We then derive the first circulation condition of the E-plane small and large gap junction in Section 3. The second circulation condition of the magnetised E-plane circulator is discussed in Section 4. We then calculate the peak power handling of the E-plane circulator in Section 5, and show that the peak power handling of the large gap is greater than the E-plane small gap and an H-plane circulator optimised at the same centre frequency.

2 | Geometry of the Large Gap E-Plane Junction Under Study

The E-plane junction circulator consists of one or two quarter-wavelength long gyromagnetic prisms or cylindrical resonators on one or both narrow waveguide walls at the junction of three rectangular waveguides. The E-plane resonator under study is shown at Figure 1a with the physical dimensions labelled in Figure 1b. Ferrite resonators of diameter $2R$, thickness L and permittivity ϵ_f are mounted on circular metallic pedestals of height $(a - 2L - 2S)/2$ and diameter $2R_1$. The gap between the resonators is $2S$. In practice, rectangular pedestals of length R_1 and width $W = b$ are often used instead of circular pedestals to avoid the possibility of a spike in the passband.

The normalised variables of the junction are given by R/L , S/L and R_1/R . A gap factor (Q_{eff}) is defined by the following equation:

$$Q_{\text{eff}} = \frac{L}{L + S} \quad (1)$$

The normalised radial wavenumber of the resonator k_0R is defined in terms of the free space wavelength k_0 and is arbitrarily fixed midway between the cutoff number of the dominant mode and the first higher order mode of the resonator. The value of k_0R is defined by the following equation:

$$k_0R = \frac{2\pi R}{\lambda_0} \quad (2)$$

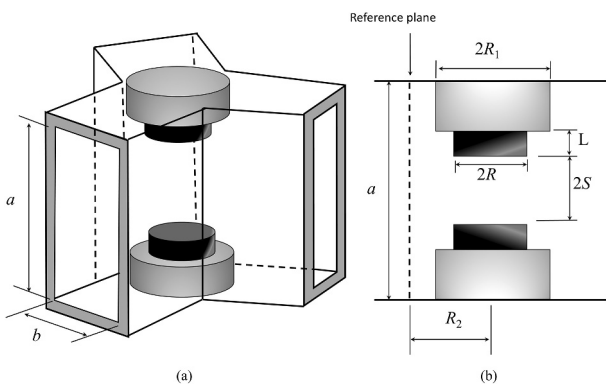


FIGURE 1 | (a) Schematic representation of the E-plane wye junction with cylindrical resonators. (b) Side view showing dimensions of the junction.

For a quarter wavelength long cylindrical resonator with a perfect magnetic wall, k_cR and the aspect ratio R/L are given by the following equation:

$$k_cR = 1.84 \quad (3a)$$

$$\frac{R}{L} = \left(\frac{2}{\pi}\right) \sqrt{(k_0R)^2 \epsilon_f - (k_cR)^2} \quad (3b)$$

When the reference plane position R_2 is defined, the normalised variables along with k_0 and ϵ_f are sufficient to solve the first circulation condition which are set to define the physical dimensions of the junction [27].

3 | First Circulation Condition of the E-Plane Small and Large Gap Junction by Adjusting the Eigenvalues

The E-plane junction differs from its H-plane counterpart in that two pairs of output waves are 180° out-of-phase [34–38]. The required eigenvalues are found by first setting the determinant of $S - \lambda I$ to zero where S is the scattering matrix, λ the eigenvalue and I the identity matrix as outlined in Appendix A [39–45]. Solving the characteristic equation leads to the eigenvalues ρ_1 , ρ_2 and ρ_3 where ρ_1 is the in-phase eigenvalue and ρ_2 and ρ_3 are the counter-rotating eigenvalues.

For a symmetric 3-port reciprocal junction, the counter-rotating eigenvalues are degenerate, and the reflection eigenvalue angles φ_1 and $\varphi_{2,3}$ may be written as a linear combination of the S parameters as follows:

$$\rho_1 = 1 \exp(j\varphi_1) = S_{11} - 2S_{12} \quad (4a)$$

$$\rho_{2,3} = 1 \exp(j\varphi_{2,3}) = S_{11} + S_{12} \quad (4b)$$

The adjustments of φ_1 and $\varphi_{2,3}$ define the first circulation condition and are the objects of optimization. As in the case of the H-plane junction, the required angles at the input terminals for the small gap E-plane are as follows:

$$\varphi_1 = \pi, 0 \text{ rad} \quad (5a)$$

$$\varphi_{2,3} = 0, \pi \text{ rad} \quad (5b)$$

which satisfy the passband condition $S_{11} = -1/3$ and $S_{21} = \pm 2/3$. The required angles of the large gap E-plane are as follows:

$$\varphi_1 = 0, \pi \text{ rad} \quad (6a)$$

$$\varphi_{2,3} = 0, \pi \text{ rad} \quad (6b)$$

which satisfy the stopband condition $S_{11} = \pm 1$ and $S_{21} = 0$. The corresponding eigenvalue diagrams are shown in Figure 2.

For the small gap E-plane junction, a practical solution for the in-phase reflection eigenvalue is an electric wall at the input terminal of the junction (Figure 2a). It differs from the large gap geometry that displays a magnetic wall (Figure 2c). In each case, the field associated with the corresponding eigenvector does not propagate along the axis of the resonator. The degenerate eigenvalues both have magnetic walls. The counter-rotating

eigenvectors impose circularly polarised magnetic fields on the inner open faces of the resonators that propagate along the axis and upon reflection at the outer short-circuited faces of the resonators.

The first circulation condition is obtained using an algorithm similar to that shown in Ref. [46, 47]. Once the reference plane is defined (R_2) the physical variables of the junction (R, L and S) are found at the intersection of two curves (q_1 and $q_{2,3}$) that defines the relationship between the radial wavenumber (k_0R) and aspect ratio of the junction (Q_{eff}) for the in-phase (ρ_1) and counter-rotating ($\rho_{2,3}$) eigenvalues. The variable parameters are $k_0R, \epsilon_f, R/L, R_1/R$ and R_2/R and the unknown variable is Q_{eff} .

Although the small gap geometry was tackled in Ref. [27], it is reproduced here for the sake of completeness. The eigenvalues ($\rho_1 = -1; \rho_{2,3} = +1$) and S-parameters of one solution displaying a passband at 13.25 GHz are plotted in Figures 3 and 4.

Figure 5 shows the eigenvalue angles with respect to the gap factor Q_{eff} for two sets of large gap variables. The S parameters of two solutions ($\varphi_{1,2,3} = 0$) display a stopband as shown in Figure 6. In both cases, the b dimension of the pedestal is reduced to suppress a possible mode in the in-phase eigenvalue. The eigenvalues ($\rho_{1,2,3} = +1$) of one solution are plotted in Figure 7.

One may obtain the same frequency response with $\rho_{1,2,3} = -1$ by placing the reference plane at $R_2/R = 0.529$.

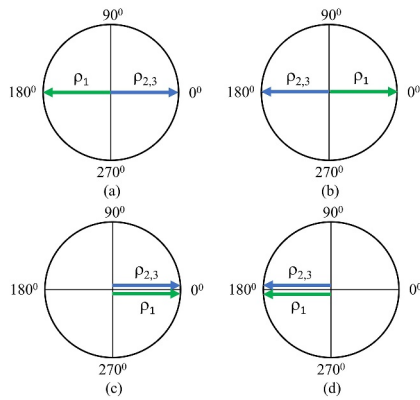


FIGURE 2 | Computed eigenvalue diagrams of small gap (a) $\rho_1 = -1, \rho_{2,3} = +1$ (b) $\rho_1 = +1, \rho_{2,3} = -1$ and large gap (c) $\rho_{1,2,3} = +1$ (d) $\rho_{1,2,3} = -1$ solutions.

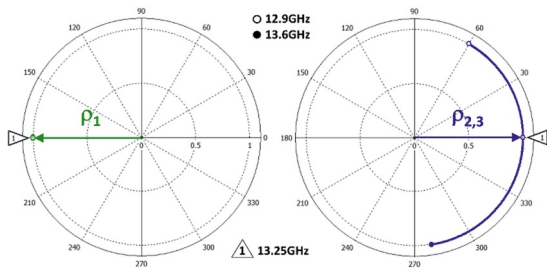


FIGURE 3 | Computed eigenvalues of small gap E-plane junction ($k_0R = 0.6715, \epsilon_f = 15, R/L = 1, Q_{\text{eff}} = 0.50, R_1/R = 1.5, R_2/R = 0.939$).

Figure 8 shows a photograph of a large gap E-plane and Figure 9 compares the simulated and measured frequency response. This unit displays a stopband near 13.8 GHz. A

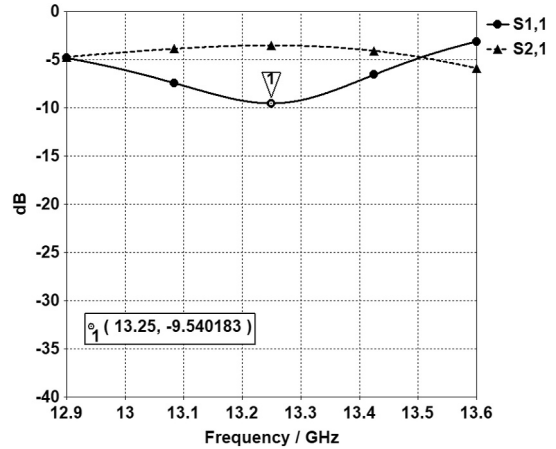


FIGURE 4 | Full-wave simulation of the passband frequency response of E-plane junction small gap solution.

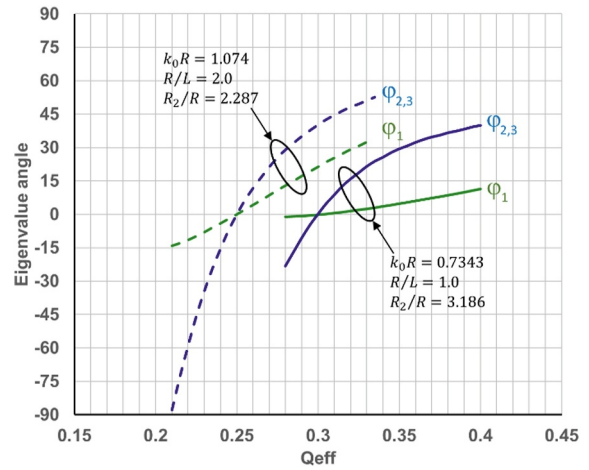


FIGURE 5 | Computed eigenvalue angles for two large gap solutions at 13.25 GHz ($\epsilon_f = 15; R_1/R = 1.5; b_{\text{pedestal}} = 0.85 * b$).

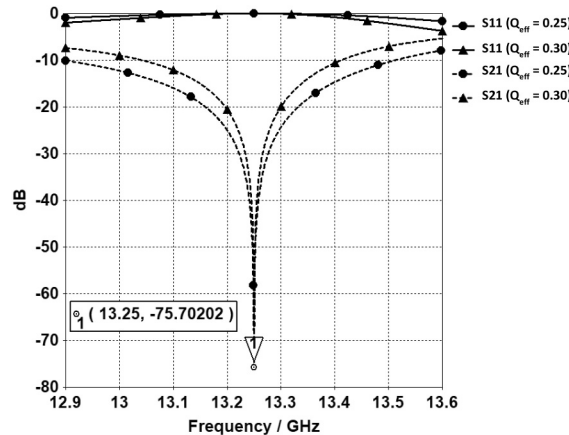


FIGURE 6 | Computed stopband frequency response of two E-plane large gap solutions ($Q_{\text{eff}} = 0.25; Q_{\text{eff}} = 0.30$).

mode suppressor was used to push an unwanted spike out of the passband.

4 | Second Circulation Condition of the Magnetised E-Plane Circulator

The second circulation condition is obtained by replacing the dielectric resonator with a gyromagnetic one and magnetising the junction. This has the effect of splitting the degeneracy between the counter-rotating eigenvalues and produces a large gap frequency response as shown in Figure 10. The eigenvalues are displaced by 120° as illustrated in Figure 11a.

The eigenvalue diagram of Figure 11b is produced by magnetising the small gap solution at Figure 3. It is worth noting the direction of circulation is reversed as shown in Figure 12. The bandwidth of the large gap is a factor of 1.8 larger than the small gap at the 20 dB return loss level.

Figure 13 shows a cross-section view of the electric field pattern near the centre frequency, for the large gap and small gap E-plane junction. The input power is set to 1W at port 1.

5 | Power Handling of the E and H-Plane Junction Circulators

On the one hand, the average power handling of the circulator depends upon the thermal gradient across the ferrite puck and the amount of heat one can extract from the circulator body, assuming the thermal drift of the magnetization of the ferrite and magnets can be controlled, to avoid detuning the junction. One could determine the temperature profile across the ferrites through numerical simulation, for a given cooling system configuration, and estimate the average power handling or

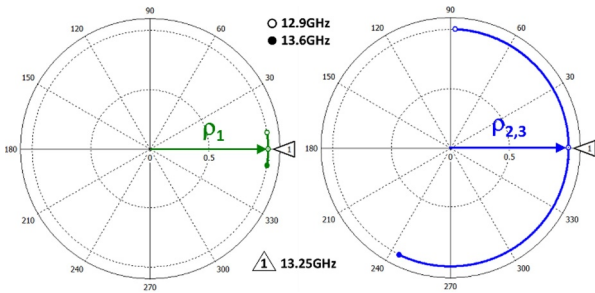


FIGURE 7 | Computed eigenvalues of E-plane large gap solution ($k_0R = 0.7343$; $\epsilon_f = 15$; $R/L = 1$; $Q_{\text{eff}} = 0.30$; $R_1/R = 1.5$; $R_2/R = 3.186$).

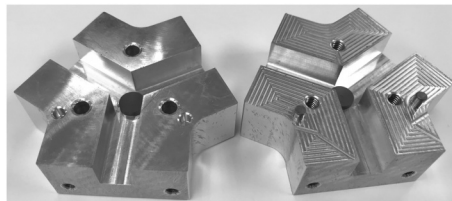


FIGURE 8 | Photograph of fabricated WR75 large gap E-plane ($k_0R = 1.0459$, $\epsilon_f = 14.6$, $R/L = 2$, $Q_{\text{eff}} = 0.23$, $R_1/R = 1.1$, $R_2/R = 1.5$).

directly measure the average power handling of the circulator unit.

On the other hand, the peak power handling depends upon the maximum electric field in the circulator junction before corona breakdown in a pressurised unit or multipaction in vacuum. The peak power handling also depends on whether the ferrites are biased below or above resonance. In the former case, peak power handling may be limited by the presence of a subsidiary resonance, because of the generation of spinwaves [48, 49] which is not the case above resonance.

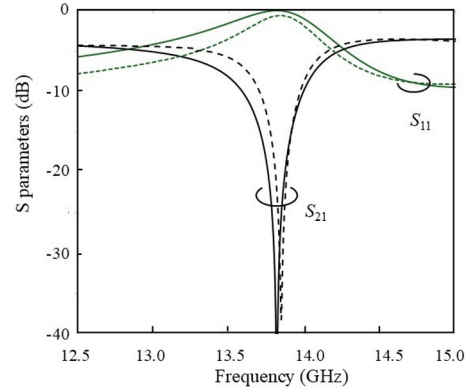


FIGURE 9 | Comparison between measured (dashed) and computed (solid) frequency response of WR75 E-plane large gap junction. ($k_0R = 1.0459$, $\epsilon_f = 14.6$, $R/L = 2$, $Q_{\text{eff}} = 0.23$, $R_1/R = 1.1$, $R_2/R = 1.5$).

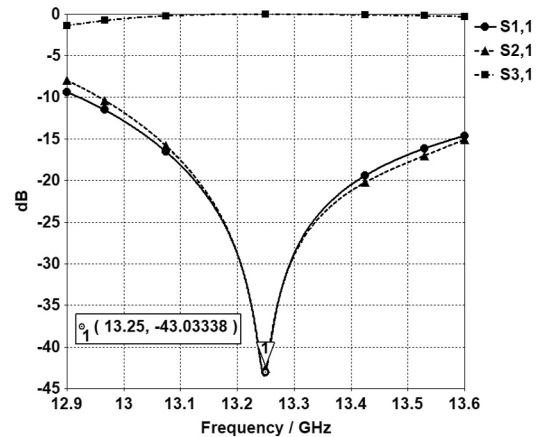


FIGURE 10 | Computed full-wave simulated frequency response of large gap E-plane circulator ($Q_{\text{eff}} = 0.30$). The curves for S_{21} and S_{13} (isolation) are superimposed and therefore cannot be distinguished.

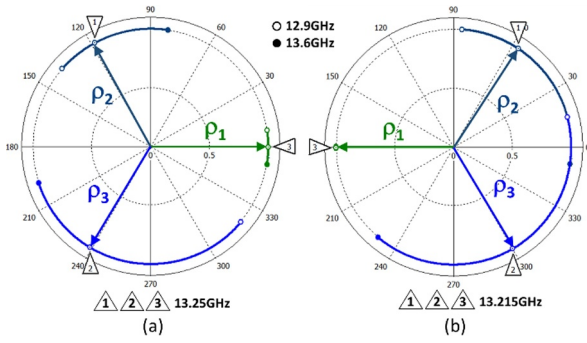


FIGURE 11 | Computed eigenvalue diagrams of magnetised E-plane (a) large gap ($Q_{\text{eff}} = 0.30$, $M_s = 800$ mT) and (b) small gap ($Q_{\text{eff}} = 0.50$, $M_s = 350$ mT) circulator.

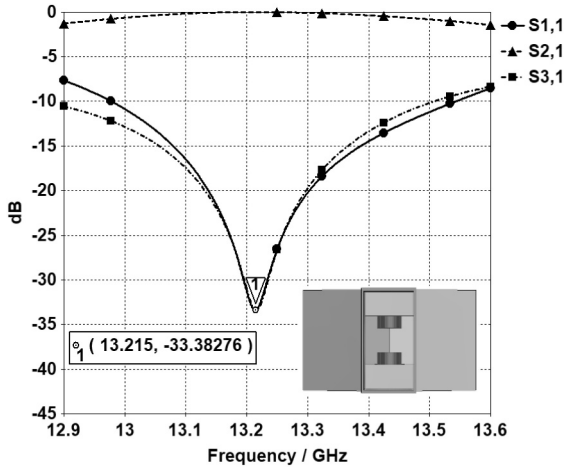


FIGURE 12 | Computed frequency response of the magnetised E-plane small gap circulator ($Q_{\text{eff}} = 0.50$). The curves for S_{12} (isolation) and S_{31} are superimposed and therefore cannot be distinguished.

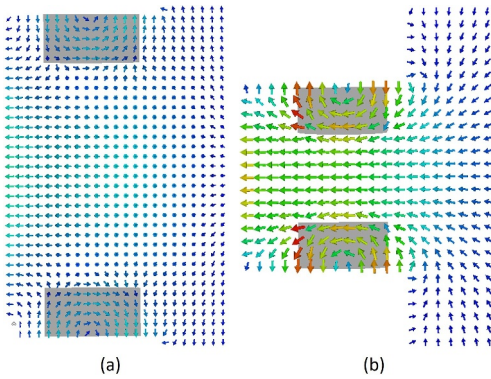


FIGURE 13 | Simulation of the electric field pattern near the centre frequency with input power 1W at port 1. (a) Large gap ($Q_{\text{eff}} = 0.30$, $E_{\text{max}} = 7.5\text{kV/m}$) and (b) small gap ($Q_{\text{eff}} = 0.50$, $E_{\text{max}} = 12.1\text{kV/m}$).

The circulators were analysed under a full short circuit condition at the output port, to determine the maximum peak power handling before corona breakdown. The position of the short was varied until a maximum electric field was observed between

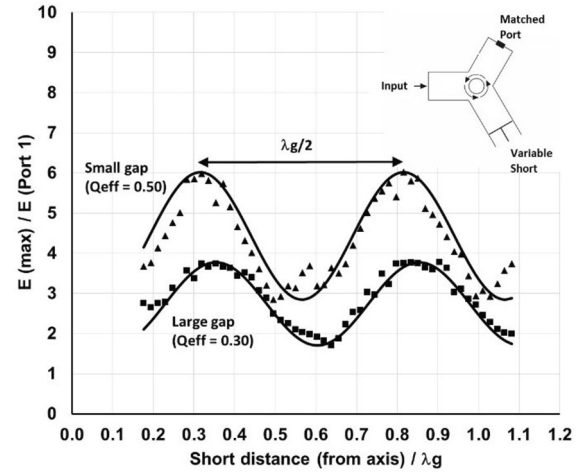


FIGURE 14 | Computed electric field handling of the small gap (triangles) and large gap (squares) junction circulators as a function of the short-circuit position at the output port. The solid lines are a guide to the eye.

the ferrites as shown in Figure 14. The period between the maxima is about $\lambda_g/2$, where λ_g is the guided wavelength. The ratio of the maximum electric fields between the large and small gap circulators suggests that the power handling of the large gap is a factor of 2.54 ($6.02^2/3.78^2$) greater than that of the small gap. The peak power handling of the circulators was analysed using SPARK3D software [50]. Assuming a dry air pressure of 3 bars and a temperature of 373 K a corona breakdown ratio of 2.58 was obtained between the large gap (556 kW) and small gap (216 kW) solutions. Positioning the short at the minimum E-field locations gives a power handling of 1.96 MW and 686 kW for the large and small gaps (ratio = 2.86), respectively. With matched loads at each output port, the breakdown of the large and small gaps is 904 and 518 kW (ratio = 1.75), respectively. The breakdown power of the WR75 waveguide feeds is 5.8 MW with a matched load.

For comparison, the breakdown power of a quarter-wave coupled H-plane junction with matched loads is 148 kW. The analysed design uses a single ferrite, and its frequency response is shown at Figure 15 [27].

Table A1 summarises the performance of the E-plane circulators available from the literature. It is presented at Appendix B to facilitate reading of the manuscript.

The E-plane junction circulator dealt with here is a below resonance circulator, and as such could be limited by the presence of a subsidiary resonance. However, one may design an above resonance large gap E-plane junction circulator to avoid the limitations introduced by the excitation of spinwaves. Indeed, Carignan and Tsounis fabricated and measured an above resonance 5 MW peak power and 2.5 kW average power handling circulator at 2.998 GHz [9]. A larger average power circulator (5 MW peak and 25 kW average) was obtained at 2.998 GHz using an above resonance 4-port differential phase-shift circulator [9]. Here, the peak power handling before corona breakdown is calculated to be 556 kW at 13.25 GHz for an E-plane large gap circulator, however, the specific design of

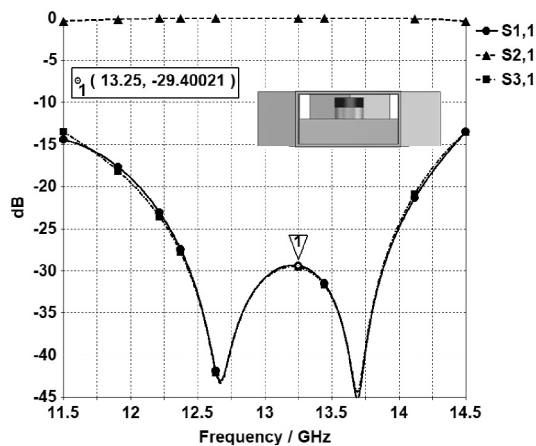


FIGURE 15 | Full-wave simulated frequency response of quarter-wave coupled H-plane circulator ($Q_{\text{eff}} = 0.744$). The curves for S_{12} (isolation) and S_{31} are superimposed and therefore cannot be distinguished.

either above resonance circulator, or a below resonance circulator operating between the main and subsidiary resonances, is outside the scope of this work.

Razavipour et al. designed a dual band E-plane circulator [31]. The authors use a pair of triangular ferrite posts in combination with a dielectric spacer to improve the bandwidth. While no power handling figures are presented, the dielectric sleeve could, in theory, improve the peak power handling of the circulator provided there are no air gaps between the ferrite and the dielectric. In contrast, the ferrite triangular post thickness could limit the average power handling of the circulator.

Deng et al. have designed a 4-port E-plane junction circulator using X-shaped ferrites at 8.5 GHz with a bandwidth of 11.8% [32]. The measured peak power level was 28 kW but the authors anticipate a peak power level of 55 kW before nonlinearity and 99.7 kW before corona breakdown.

The E-plane junction circulator presented here is degree-1, and therefore has an inherently smaller bandwidth than the circulators mentioned above. However, the use of a quarter-wave transformer, to obtain a degree-2 E-plane junction, would improve the bandwidth of the circulator. A ferrite-dielectric stack in the E-plane, as used by DeCamp and True [8] or Longley [11], could also broaden the band of operation. The extent to which the bandwidth may be improved needs to be evaluated.

6 | Conclusion

A characteristic of the E-plane circulator is that it displays neighbouring small and large gap solutions for its first circulation condition. The paper has employed an eigenvalue approach to compare the passband and stopband characteristics of both cases and has demonstrated that the power level before corona breakdown of the corresponding large gap circulator is significantly improved compared with the small gap and H-plane solutions.

The design of a quarter-wave coupled large gap E-plane junction circulator, for improved bandwidth, is under consideration.

Author Contributions

Joseph Helszajn: conceptualisation, formal analysis, supervision, validation, writing – original draft. **Louis-Philippe Carignan:** conceptualisation, software, validation, writing – original draft, writing – review and editing. **Mark McKay:** software, validation, writing – original draft, writing – review and editing. **Bill Tsounis:** supervision, validation. **Ke Wu:** supervision, validation, writing – original draft, writing – review and editing.

Acknowledgements

The authors would like to thank Steve Dubé, from PolyGrames Research Center, for machining the circulator bodies.

Conflicts of Interest

The authors declare no conflicts of interest.

Data Availability Statement

Data are available on request from the authors.

References

1. S. Yoshida, “E-Type T Circulator,” *Proceedings of the IRE* 47 (1959): 2018.
2. H. N. Chait and T. R. Curry, “Y Circulator,” *Journal of Applied Physics* 30, no. 4 (1959): S152–S153, <https://doi.org/10.1063/1.2185863>.
3. L. E. Davis and S. R. Longley, “E-Plane 3-Port X-Band Waveguide Circulators (Correspondence),” *IEEE Transactions on Microwave Theory and Techniques* 11, no. 5 (September 1963): 443–445, <https://doi.org/10.1109/tmtt.1963.1125696>.
4. G. Buchta, “Miniaturized Broadband E-Tee Circulator at X-Band,” *Proceedings of the IEEE* 54, no. 11 (November 1966): 1607–1608, <https://doi.org/10.1109/proc.1966.5221>.
5. M. Omori, “An Improved E-Plane Waveguide Circulator,” in *1968 G-MTT International Microwave Symposium* (IEEE, May 1968), 228–236.
6. J. W. McGowan and W. H. Wright, “A High Power, Y Junction, E-Plane Circulator,” in *1967 G-MTT International Microwave Symposium Digest* (IEEE, May 1967), 85–87.
7. W. H. Wright and J. W. McGowan, “High-Power Y-Junction E-Plane Circulator (Correspondence),” *IEEE Transactions on Microwave Theory and Techniques* 16, no. 8 (August 1968): 557–559, <https://doi.org/10.1109/tmtt.1968.1126742>.
8. E. E. DeCamp and R. M. True, “1-MW Four-Port E-Plane Junction Circulator (Correspondence),” *IEEE Transactions on Microwave Theory and Techniques* 19, no. 1 (January 1971): 100–103, <https://doi.org/10.1109/tmtt.1971.1127455>.
9. L. P. Carignan and V. Tsounis, “High Peak Power Circulators,” in *International Workshop on Multipactor, Corona and Passive Intermodulation (MULCOPIM)* (ESA/ESTEC, 2017), 173–179.
10. L. P. Carignan and V. Tsounis, “E-Plane Waveguide Circulator for Operation Above Magnetic Resonance, WO 2016/187691 A1,” (2016).
11. S. R. Longley, “Experimental 4-Port E-Plane Junction Circulators (Correspondence),” *IEEE Transactions on Microwave Theory and Techniques* 15, no. 6 (June 1967): 378–380, <https://doi.org/10.1109/tmtt.1967.1126477>.

12. J. Helszajn, *Waveguide Junction Circulators, Theory and Practice* (John Wiley and Sons, 1998).
13. J. Helszajn and M. McDermott, "Mode Chart for E-Plane Circulators (Correspondence)," *IEEE Transactions on Microwave Theory and Techniques* 20, no. 2 (February 1972): 187–188, <https://doi.org/10.1109/tmtt.1972.1127710>.
14. M. E. El-Shandwily, A. A. Kamal, and E. A. F. Abdallah, "General Field Theory Treatment of E-Plane Waveguide Junction Circulators - Part I: Full-Height Ferrite Configuration," *IEEE Transactions on Microwave Theory and Techniques* 25, no. 9 (September 1977): 784–793, <https://doi.org/10.1109/tmtt.1977.1129212>.
15. M. E. El-Shandwily, A. A. Kamal, and E. A. F. Abdallah, "General Field Theory Treatment of E-Plane Waveguide Junction Circulators - Part II: Two-Disk Ferrite Configuration," *IEEE Transactions on Microwave Theory and Techniques* 25, no. 9 (September 1977): 794–803, <https://doi.org/10.1109/tmtt.1977.1129213>.
16. I. Alexander and K. Flett, "Design and Development of High Power Ku-Band Junction Circulators," *IEEE Transactions on Magnetics* 13, no. 5 (September 1977): 1255–1257, <https://doi.org/10.1109/tmag.1977.1059530>.
17. M. Brass and C. Schieblich, "E-Type Circulator for Fin Lines," *Electronics Letters* 17, no. 19 (October 1981): 701–702, <https://doi.org/10.1049/el:19810491>.
18. C. Schieblich, "Mode Charts for Magnetized Ferrite Cylinders," *IEEE Transactions on Microwave Theory and Techniques* 37, no. 10 (October 1989): 1555–1561, <https://doi.org/10.1109/22.41001>.
19. K. Solbach, "Equivalent Circuit Representation for the E-Plane Circulator," *IEEE Transactions on Microwave Theory and Techniques* 30, no. 5 (May 1982): 806–809, <https://doi.org/10.1109/tmtt.1982.1131141>.
20. U. Goebel and C. Schieblich, "A Unified Equivalent Circuit Representation for H- and E-Plane Junction Circulators," in *1983 13th European Microwave Conference* (IEEE, September 1983), 803–808.
21. J. Helszajn and J. Sharp, "Dielectric and Permeability Effects in HE_{1,1,1/2} Open Demagnetized Ferrite Resonators," *IEE Proc.* 133, no. H (1986): 271–276, <https://doi.org/10.1049/ip-h-2.1986.0048>.
22. J. Helszajn, "Complex Gyrotator Circuit of an Evanescent-Mode E-Plane Junction Circulator Using H-Plane Turnstile Resonators," *IEEE Transactions on Microwave Theory and Techniques* 35, no. 9 (September 1987): 797–806, <https://doi.org/10.1109/tmtt.1987.1133755>.
23. J. Helszajn and S. Cheng, "Aspect Ratio of Open Resonators in Design of Evanescent Mode E-Plane Circulators," *IEE Proceedings H - Microwaves, Antennas and Propagation* 137, no. 1 (February 1990): 55–60, <https://doi.org/10.1049/ip-h-2.1990.0010>.
24. S. Cheng, "Mode Charts of E-Plane Circulators," in *IEE Colloquium on Ferrite Materials* (Devices and Applications, 1989), 4/1–4/5.
25. A. C. Gravina, "E-Plane Circulators for Integrated Millimetric Sub-Systems," in *IEE Colloquium on Ferrite Materials, Devices and Applications* (IET, 1989), 9/1–9/5.
26. M. Caplin, W. D'Orazio, and J. Helszajn, "First Circulation Condition of E-Plane Circulator Using Single-Prism Resonator," *IEEE Microwave and Guided Wave Letters* 9, no. 3 (March 1999): 99–101, <https://doi.org/10.1109/75.761673>.
27. J. Helszajn, *Microwave Polarizers, Power Dividers, Phase Shifters, Circulators and Switches* (John Wiley and Sons, 2019).
28. K. Solbach, "E-Plane Circulators 30 Through 150 GHz for Integrated Mm-Wave Circuits," in *1983 13th European Microwave Conference* (IEEE, 1983), 163–167.
29. L. Ping and Y. Quanrang, "Millimeter Wave E-Plane Waveguide Junction Circulator," in *2002 3rd International Conference on Microwave and Millimeter Wave Technology, 2002. Proceedings. ICMMT 2002* (IEEE, 2002), 952–954.
30. K. Solbach, "94-GHz 4-Port E-Plane Junction Circulator (Short Paper)," *IEEE Transactions on Microwave Theory and Techniques* 32, no. 7 (July 1984): 722–724, <https://doi.org/10.1109/tmtt.1984.1132765>.
31. H. Razavipour, G. Askari, F. Fesharaki, and H. Mirmohammad-Sadeghi, "A New High-Power, Dual-Band, E-Plane, Ferrite Circulator," in *IEEE EUROCON 2009* (IEEE, 2009), 20–25.
32. G. Deng, L. Guo, J. Li, W. Huang, H. Shao, and T. Ba, "A Compact E-Plane Four-Port Junction Circulator," *IEEE Microwave and Wireless Components Letters* 29, no. 10 (2019): 655–658, <https://doi.org/10.1109/lmwc.2019.2937865>.
33. G. Deng, J. Li, T. Ba, et al., "Design of Compact E-Plane Differential Phase Shift Circulators," in *2018 Asia-Pacific Microwave Conference (APMC)* (IEEE, 2018), 291–293.
34. J. T. Allanson, R. Cooper, and T. G. Cowling, "The Theory and Experimental Behaviour of Right-Angled Junctions in Rectangular-Section Wave Guides," *Journal of the Institution of Electrical Engineers - Part III: Radio and Communication Engineering* 93, no. 23 (May 1946): 177–187, <https://doi.org/10.1049/ji-3-2.1946.0028>.
35. J. L. Altman, "Microwave Circuits," in *Van Nostrand Series in Electronics and Communications* (Princeton, 1964).
36. A. Casanueva, A. Leon, A. Mediavilla, and J. Helszajn, "Characteristic Planes of Microstrip and Unilateral Finline Tee-Junctions," in *Progress in Electromagnetics Research Symposium Proceedings* (IEEE, August 2013), 173–179.
37. J. Helszajn, M. Caplin, J. Frenna, and B. Tsounis, "Characteristic Planes and Scattering Matrices of E and H-Plane Waveguide Tee Junctions," *IEEE Microwave and Wireless Components Letters* 24, no. 4 (April 2014): 209–211, <https://doi.org/10.1109/lmwc.2013.2295229>.
38. J. Helszajn, "The Electrically Symmetrical E-Plane Waveguide Tee Junction at the Dicke and Altman Planes," *IEEE Transactions on Microwave Theory and Techniques* 64, no. 3 (March 2016): 715–723, <https://doi.org/10.1109/tmtt.2016.2521651>.
39. Y. Akaiwa, "Operation Modes of a Waveguide Y Circulator (Short Papers)," *IEEE Transactions on Microwave Theory and Techniques* 22, no. 11 (November 1974): 954–960, <https://doi.org/10.1109/tmtt.1974.1128392>.
40. Y. Akaiwa, "A Numerical Analysis of Waveguide H-Plane Y-Junction Circulators With Circular Partial-Height Ferrite Post," *Journal of the Institute of Electronics and Communication Engineers of Japan E61*, no. 11 (1978): 609–617.
41. C. G. Montgomery, R. H. Dicke, and E. M. Purcell, "Principles of Microwave Circuits," in *M.I.T. Radiation Lab. Series*, Vol. VIII (McGraw-Hill Book Company, 1948), 432.
42. B. A. Auld, "The Synthesis of Symmetrical Waveguide Circulators," *IRE Transactions on Microwave Theory and Techniques* 7, no. 2 (April 1959): 238–246, <https://doi.org/10.1109/tmtt.1959.1124688>.
43. B. Owen and C. E. Barnes, "The Compact Turnstile Circulator," *IEEE Transactions on Microwave Theory and Techniques* 18, no. 2 (December 1970): 1096–1100, <https://doi.org/10.1109/TMTT.1970.1127417>.
44. B. Owen, "The Identification of Modal Resonances in Ferrite Loaded Waveguide Y-Junctions and Their Adjustment for Circulation," *Bell System Technical Journal* 51, no. 3 (March 1972): 595–627, <https://doi.org/10.1002/j.1538-7305.1972.tb01938.x>.
45. J. Helszajn, "The Adjustment of the M-Port Single- Junction Circulator," *IEEE Transactions on Microwave Theory and Techniques* 18, no. 10 (October 1970): 705–711, <https://doi.org/10.1109/tmtt.1970.1127333>.
46. J. Helszajn, "A Finite-Element Algorithm for the Adjustment of the First Circulation Condition of the Turnstile Waveguide Circulator," *IEEE Transactions on Microwave Theory and Techniques* 60, no. 10 (October 2012): 3079–3087, <https://doi.org/10.1109/tmtt.2012.2209452>.

47. J. Helszajn, L. Carignan, and J. Sharp, "Calibration and Adjustments of Degree-1 and -2 Re-Entrant Turnstile Circulators Using a Partially Recessed Quarter-Wave Long Dielectric Resonator," *IET Microwaves, Antennas and Propagation* 10, no. 1 (2016): 1–7.

48. H. Suhl, "The Nonlinear Behavior of Ferrites at High Microwave Signal Levels," *Proceedings of the IRE* 44, no. 10 (1956): 1270–1284, <https://doi.org/10.1109/jrproc.1956.274950>.

49. M. Chen and C. Patton, *Spin Wave Instability Processes in Ferrites, Chap. 3 in Nonlinear Phenomena and Chaos in Magnetic Materials* (World Scientific Connect, 1994).

50. Simulia SPARK3D, "Dassault Systems," <https://www.3ds.com/products/simulia/spark3d>.

Appendix A

The scattering matrix of the E-plane geometry differs from that of the H-plane one in that $S_{13} = -S_{23}$ and $S_{31} = -S_{21}$. The scattering matrix of a symmetric 3-port reciprocal E-plane junction is given by the following equation:

$$\bar{S} = \begin{bmatrix} S_{11} & S_{12} & -S_{12} \\ S_{12} & S_{11} & S_{12} \\ -S_{12} & S_{12} & S_{11} \end{bmatrix} \quad (\text{A1})$$

The eigenvalues ρ_i , with $i = 1, 2$ and 3 , of the symmetric reciprocal E-plane junction may be obtained by solving the following equation:

$$\det \begin{bmatrix} S_{11} - \rho_i & S_{12} & -S_{12} \\ S_{12} & S_{11} - \rho_i & S_{12} \\ -S_{12} & S_{12} & S_{11} - \rho_i \end{bmatrix} = 0 \quad (\text{A2})$$

Setting the determinant equal to zero gives the characteristic equation, from which we extract the eigenvalues. The corresponding eigen-vectors U_i with $i = 1, 2$ and 3 satisfy the following equation:

$$\bar{S}U_i = \rho_i U_i \quad (\text{A3})$$

with

$$U_1 = \frac{1}{\sqrt{3}} \begin{bmatrix} 1 \\ -1 \\ 1 \end{bmatrix}, \quad (\text{A4})$$

$$U_2 = \frac{1}{\sqrt{3}} \begin{bmatrix} 1 \\ -\exp\left(j\frac{2\pi}{3}\right) \\ \exp\left(-j\frac{2\pi}{3}\right) \end{bmatrix} \quad (\text{A5})$$

$$U_3 = \frac{1}{\sqrt{3}} \begin{bmatrix} 1 \\ -\exp\left(-j\frac{2\pi}{3}\right) \\ \exp\left(j\frac{2\pi}{3}\right) \end{bmatrix} \quad (\text{A6})$$

Appendix B

Table A1 summarises the results from the literature on E-plane circulators. When available, the insertion loss (I.L.), return loss (R.L.), isolation (Isol.), centre frequency (f_0), bandwidth ($\Delta\omega/\omega_0$), peak power handling and type of circulator are indicated. The table is sorted by increasing order of centre frequency f_0 .

TABLE A1 | Summary of the performance of the E-plane circulators from literature.

Reference	I.L. (dB)	R.L. (dB)	Isol. (dB)	f_0 (GHz)	$\Delta\omega/\omega_0$ (%)	Peak power (kW)	Notes
[9]	< 0.15	> 28	> 28	2.998	3	5000	3-port junction and a pair of circular ferrites (2500 W average power)
[8]	0.5	18.5	15	3.14	15	1000	4-port junction and a pair of circular ferrites (1000 W average power)
[5]	0.1	N.A.	30	4.05	12.3	N.A.	3-port junction, single ferrite post and metallic plugs for tuning
[31]	0.1	20	20	8.2 & 10.4	N.A.	N.A.	3-port junction and a pair of triangular ferrite posts
[32]	0.3–0.6	18	17	8.5	11.8	55	4-port junction and a pair of X-shaped ferrites (400 Hz repetition rate, 1 μ sec pulse width)
[33]	0.3–0.5	20	15	8.75	11.4	N.A.	4-port differential phase shift circulator
[4]	0.5	16	20	9	11.1	N.A.	3-port junction and single circular ferrite
[11]	< 0.7	24	20	9.0	6	60	4-port junction and a pair of circular ferrites (40 W average power)
[6, 7]	0.6–0.8	N.A.	15	9.375	0.64	500	3-port junction and a pair of circular ferrites (600 W average power)
[3]	0.5	18	20	9.6	10.4	N.A.	3-port junction and a pair of circular ferrites
[3]	0.5	19	15	10.2	11.8	N.A.	3-port junction and a pair of circular ferrites
[3]	0.5	17	20	10.5	9.5	N.A.	3-port junction and a pair of triangular ferrites
This work	0.1	20	20	13.25	3	556	3-port junction and a pair of circular ferrites
[29]	< 1	N.A.	15	35	2.8	N.A.	3-port junction, and a single ferrite
[30]	0.65	15	15	94	1	N.A.	4-port junction and a single ferrite
[28]	0.5	N.A.	20	94	1.3	N.A.	3-port junction and a single ferrite
[28]	1	N.A.	20	145	1.7	N.A.	3-port junction and a single ferrite